

Over 65% sunlight absorption in a 1 μm Si slab with hyperuniform texture

Nasim Tavakoli

AMOLF

Richard Spalding

University of Surrey

Pepijn Koppejan

AMOLF

Georgio Gkantzounis

University of Surrey

Chenglong Wang

University of Surrey

Ruslan Röhrich

AMOLF

Evgenia Kontoleta

AMOLF

A. Femius Koenderink

AMOLF <https://orcid.org/0000-0003-1617-5748>

Riccardo Sapienza

Imperial College London <https://orcid.org/0000-0002-4208-0374>

Marian Florescu

University of Surrey <https://orcid.org/0000-0001-6278-9164>

Esther Alarcon-Llado (✉ e.alarconllado@amolf.nl)

AMOLF <https://orcid.org/0000-0001-7317-9863>

Article

Keywords: Flexible Solar Cells, Ultrathin Crystalline Silicon Cells, Hyperuniform Nanostructuring

Posted Date: September 16th, 2020

DOI: <https://doi.org/10.21203/rs.3.rs-69198/v1>

License:   This work is licensed under a Creative Commons Attribution 4.0 International License.

[Read Full License](#)

Version of Record: A version of this preprint was published at ACS Photonics on March 22nd, 2022. See the published version at <https://doi.org/10.1021/acsp Photonics.1c01668>.

Over 65% sunlight absorption in a 1 μm Si slab with hyperuniform texture

Nasim Tavakoli,[†] Richard J. Spalding,[‡] Pepijn Koppejan,[†] Georgios Gkantzounis,[‡]
Chenglong Wan,[‡] Ruslan Röhrich,^{†,¶} Evgenia Kontoleta,[†] A. Femius Koenderink,[†]
Riccardo Sapienza,[§] Marian Florescu,^{*,‡} and Esther Alarcon-Llado^{*,†}

[†]*Center for Nanophotonics, AMOLF, Science Park 104, NL1098XG, Amsterdam, The Netherlands*

[‡]*Department of Physics, Advanced Technology Institute, University of Surrey, Surrey, UK*

[¶]*Advanced Research Center for Nanolithography, Science Park 106, NL1098XG, Amsterdam, The Netherlands*

[§]*The Blackett Laboratory, Department of Physics, Imperial College London, London SW7 2BW, United Kingdom*

E-mail: m.florescu@surrey.ac.uk; e.alarconllado@amolf.nl

Abstract

Thin, flexible and invisible solar cells will be an ubiquitous technology in the near future. Ultrathin crystalline silicon (c-Si) cells capitalise on the success of bulk silicon cells while being light-weight and mechanically flexible, but suffer from poor absorption and efficiency. Here we present a new family of surface texturing, based on correlated disordered hyperuniform patterns, capable of efficiently coupling the incident spectrum into the silicon slab optical modes. We experimentally demonstrate 66.5% solar light absorption in free-standing 1 μm c-Si layers by hyperuniform nanostructuring. The absorption equivalent photocurrent derived from our measurements is 26.3 mA/cm²,

11 which is far above the highest found in literature for Si of similar thickness. Considering
12 state-of-the-art Si PV technologies, the enhanced light trapping translates to a record
13 efficiency above 15%. The light absorption can potentially be increased up to 33.8
14 mA/cm² by incorporating a back-reflector and improved anti-reflection, for which we
15 estimate a photovoltaic efficiency above 21% for 1 μ m thick Si cells.

16 Micrometer-thick silicon photovoltaics (PV) promises to be the ultimate cost-effective, re-
17 liable and environmentally-friendly solution to harness solar power in urban areas and space,
18 as it combines the low cost and maturity of crystalline silicon (c-Si) manufacturing¹ with
19 the low weight and mechanical flexibility of thin films.²⁻⁴ Efficient light trapping in ultrathin
20 c-Si is of utmost importance when the film is thinner than the absorption length. Indeed,
21 due to the indirect bandgap of c-Si, inefficient absorption currently hampers the thinning of
22 Si cells below $\sim 100 \mu$ m, which is crucial to enable flexible, light weight and lower cost c-Si
23 PV.^{1,5,6} 3D nanophotonic architectures are crucial for reducing the cell thickness as conven-
24 tional anti-reflection coatings and multilayers can only prevent light reflection via impedance
25 matching of the solar cell and air, but do not extend the light paths in the Si cell that are
26 required for efficient photon absorption.⁷ Despite the fact that many works have focused on
27 nanophotonic principles for enhancing light absorption, there is still no unanimously agreed
28 best strategy for the designing of light trapping nano-textures for PV. Periodic patterning of
29 a thin slab, whether by adding plasmonic⁸⁻¹² or dielectric¹³⁻¹⁵ structures, can reduce reflec-
30 tion and simultaneously scatter light in the plane of the thin film, but generally work only
31 at discrete wavelengths and specific angle of incidence, due to the discrete crystal momenta
32 of gratings. Oppositely, disordered patterns, such as Asahi roughening or random pyramid
33 etching, scatter the light over a broad angular range and over a large range of wavelengths
34 due to the large rotational and translational symmetry, but are not tailored to match the
35 thin film.¹⁶

36 Recently, correlated disordered media have been shown to outperform random roughen-
37 ing and periodic patterning for light trapping.¹⁷⁻²⁶ Albeit many designs have been presented

38 so far, it is still an open question what the best design is and whether the optimal one
39 has already been achieved. For instance, it is not obvious if the best result is obtained
40 when starting the optimisation from a periodic or from a random structure. In contrast
41 to these heuristic optimisation methods, hyperuniformity has recently emerged as a new
42 framework to engineer light scattering and diffraction in a rational manner. Hyperuniform
43 disordered (HUD) media are statistically isotropic and possess a constrained randomness such
44 that density fluctuations on large scales behave more like those of ordered solids, rather
45 than those of conventional amorphous materials.^{27–30} HUD patterns naturally arise in many
46 physical systems, from the mass distribution in the early universe,³¹ structure of prime num-
47 bers,³² hydrodynamics,³³ structure of amorphous ices,³⁴ sheared sedimenting suspensions,³⁵
48 to wave localisation³⁶ or colloidal packing.³⁷ When translated into photonic materials, HUDs
49 exhibit large and robust photonic band gaps as in photonic crystals, but are both complete
50 and isotropic.³⁰ As a result, HUDs display allowed modes that can propagate through the
51 structure in an isotropic fashion as in random media. HUDs are a highly flexible platform
52 to control light transport, emission and absorption in unique ways, beyond the constraints
53 imposed by conventional photonic architectures,^{38–42} for the design of freeform waveguides,⁴³
54 high-quality factor resonant defects and arbitrarily high-order power splitters,^{44,45} hollow-
55 core fibers⁴⁶ and photonic bandgap polarizers⁴⁷ among others.

56 In this work we experimentally demonstrate that light absorption in a 1 μm -thick silicon
57 slab is enhanced more than twofold in the wavelength range from 400 to 1050 nm when
58 textured with optimised HUD-based patterns compared to the unpatterned slab. The re-
59 sulting absorption is the highest demonstrated so far in a Si slab as thin as 1 μm . This record
60 value is achieved by k-space engineering of HUD patterns with a tailored scattering spec-
61 trum and diffractive coupling of solar irradiation into guided modes of the Si slab. Using our
62 demonstration of light management, we investigate PV efficiency by focusing on the trade-off
63 between light trapping and increased carrier recombination given by the nanotextures. We
64 find that the effect of increased surface-induced charge carrier recombination on the open

65 circuit potential can be fully compensated by the large photo-currents. A detailed PV effi-
 66 ciency estimation reveals that efficiencies above 20% can be obtained for several optimised
 67 HUD designs and state-of-the-art Si PV technologies. This is a highly remarkable efficiency
 68 for such a thin indirect-bandgap material, which together with the fact that lower grade
 69 raw Si material can be used in such thin devices, establishes a new breakthrough in thin
 70 light-weight and flexible solar cells.

71 Light absorption in films with disordered hyperuniform patterns

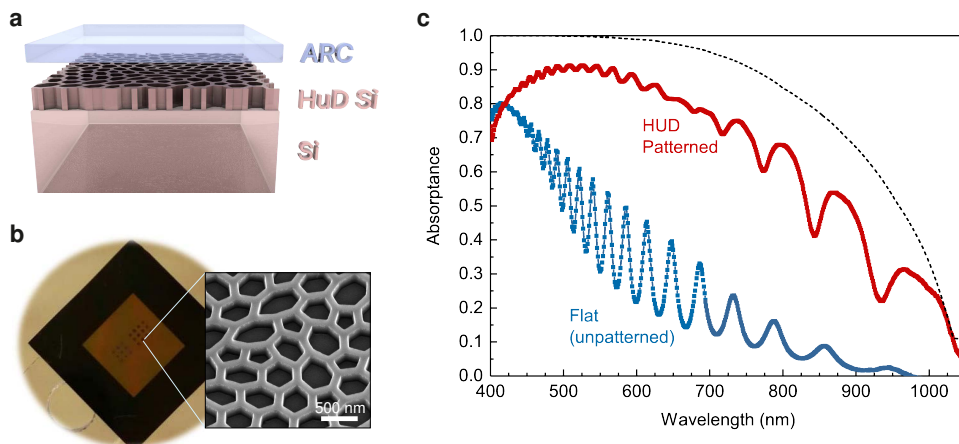


Fig. 1 Ultra-thin light absorber design. **a** Schematic representation of the ultra-thin light absorber consisting of a $1\ \mu\text{m}$ -thick silicon film with the HUD pattern on the top surface ($\sim 200\ \text{nm}$ thick) to improve light trapping. The pattern is infiltrated with a lower refractive index material (n_{LRM}), which is also used in a top flat layer, ARC, to reduce reflectance (50-100 nm in thickness). Note that the ARC layer is depicted floating above the nanopattern in the image only for clarity purposes **b** Optical image of the silicon membrane sample supported by a thick silicon frame ($1 \times 1\ \text{cm}^2$), where the textures have been fabricated. Inset: Scanning electron image of the as-fabricated Si membrane with the optimized honeycomb-like HUD network pattern. **c** Absorbance spectra measured for the Si membrane with (red) and without (blue) the HUD pattern with ARC. The membrane is suspended in air and infiltrated with a polymer resist ($n_{LRM} = 1.52$) as ARC. The dashed black line corresponds to the Lambertian limit absorption for $1\ \mu\text{m}$ Si, based on the optical properties given in Ref. 48.

72 We demonstrate the power of hyperuniform disordered (HUD) patterns for lightweight, flex-
 73 ible and efficient photovoltaics, by first focusing on the absorption properties in ultrathin
 74 ($\sim 1\ \mu\text{m}$) Si. The proposed structure for the highly efficient Si light absorber is shown in

75 Fig. 1a. It consists of a thin Si slab ($1\ \mu\text{m}$), of which the top 200 nm is patterned with
 76 an optimised HUD pattern. In this case, the pattern consists of a 2D network of Si walls,
 77 that resembles the honey-comb underlying structure in black butterfly wings.^{24,49} The Si
 78 pattern is infiltrated with a low refractive index medium by spin coating a polymer resist⁵⁰
 79 with refractive index of 1.52. While the infiltrated pattern layer is expected to also reduce
 80 reflectance due to the better index matching with air ($n_{\text{pattern}} \approx n_{\text{Si}} \cdot f + n_{\text{LRM}}(1 - f)$, with f
 81 being the Si filling fraction), an additional layer of resist on top (50 – 100 nm thick) further
 82 improves anti-reflectance, referred to as ARC. While the optical properties of the resist are
 83 not the ideal to guarantee minimal reflection, spin coating is a simple conformal fabrication
 84 method that ensures nanopattern filling and a flat top surface. Fig. 1b is a photograph
 85 of a suspended $4.8 \times 4.8\ \text{mm}^2$ Si membrane nominally $1\ \mu\text{m}$ -thick on a Si support frame
 86 before spin coating the resist. The membrane reveals a semi-transparent reddish colour
 87 owing to its small thickness and small absorption coefficient in the red and near infra-red.
 88 HUD-based patterns were fabricated on the membrane with e-beam lithography in at least
 89 $100 \times 100\ \mu\text{m}^2$ areas. These areas are clearly visible in the picture as they appear darker,
 90 highlighting the increased light trapping. A close-up scanning electron microscopy (SEM)
 91 image of the fabricated HUD network pattern on the Si suspended membrane is shown as
 92 inset.

93 We have measured the light absorption of the free-standing membrane with ARC on
 94 the unpatterned and patterned regions by using an integrating sphere microscope.^{51,52} The
 95 curves in Fig. 1c compare the light absorption as measured for the flat membrane with that
 96 of the HUD patterned membrane. The absorption spectrum of the flat membrane shows
 97 the characteristic Fabry-Pérot interferences for a $1.18\ \mu\text{m}$ thick Si slab (see Supplementary
 98 Information), with a peak in absorption at about a wavelength of 450 nm and rapidly de-
 99 creasing absorption for longer wavelengths due to the small absorption coefficient of Si in
 100 the visible and near infra-red. In contrast, the absorption in the membrane with the HUD
 101 pattern is on average 50% higher in absolute numbers for the wavelength range of 500 to 900

102 nm and it follows the Lambertian limit trend ($4n^2$ limit for 1 μm -thick Si represented by the
 103 black dashed curve), which does not take into account reflection losses. Despite the fact that
 104 the membrane sits in air (i.e. no back-reflector) and the sub-optimised ARC, the fraction
 105 of absorbed solar photons in the membrane increases from 25.5% to 66.5% by texturing the
 106 surface based on our optimised HUD design. This is the highest demonstrated absorption
 107 in a 1 μm Si absorber so far, and translates to a photocurrent of 26.3 mA/cm^2 , far above
 108 the 19.72 mA/cm^2 in the best reported cell with similar thickness.⁵³ Simulations show that
 109 a metal back reflector will increase absorption even further for the whole spectrum and inte-
 110 grated absorption can reach up to 93.4% of the Lambertian absorption. In the following, we
 111 describe the design principle and physical mechanism that induces this record in absorption.

112 **Light trapping mechanism and design optimisation**

113 As in previous works that use periodic and heuristic aperiodic structures to promote light
 114 trapping, the main mechanism by which the HUD nanostructure enhances absorption is
 115 diffraction into the absorber.^{17,54,55} In the presence of texturing, the guided modes of the
 116 thin silicon slab become leaky (quasi-guided) and can in- and out-couple to the incoming
 117 electromagnetic modes supported by the surrounding medium. The waveguide mode dis-
 118 persion for a Si slab is shown in Fig. 2a, where we note that within the spectral region of
 119 interest, c-Si exhibits strong dispersion that leads to a strong curvature of the Si light cone
 120 and significantly different absorption of the guided modes, as indicated by the color scale in
 121 Fig. 2a. The total absorption is given by summing up the coupling contributions of each
 122 mode. To maximize sunlight absorption in the slab we need to couple efficiently to these
 123 lossy modes that exist for k_{\parallel} above the light-cone of air (*lower black thick curve*), for a broad
 124 range of wavelengths (from 350 nm to 1100 nm). Due to the large number of modes in a 1
 125 μm Si slab, a pattern structure that diffracts incident light ($k_{\parallel} = 0$ for normal incidence) to
 126 the range of k_{\parallel} from ~ 15 to $\sim 20 \mu\text{m}^{-1}$ (indicated by the two horizontal dashed lines in
 127 Fig. 2a) ensures all sunlight has a mode to couple to. However, due to the inhomogeneous

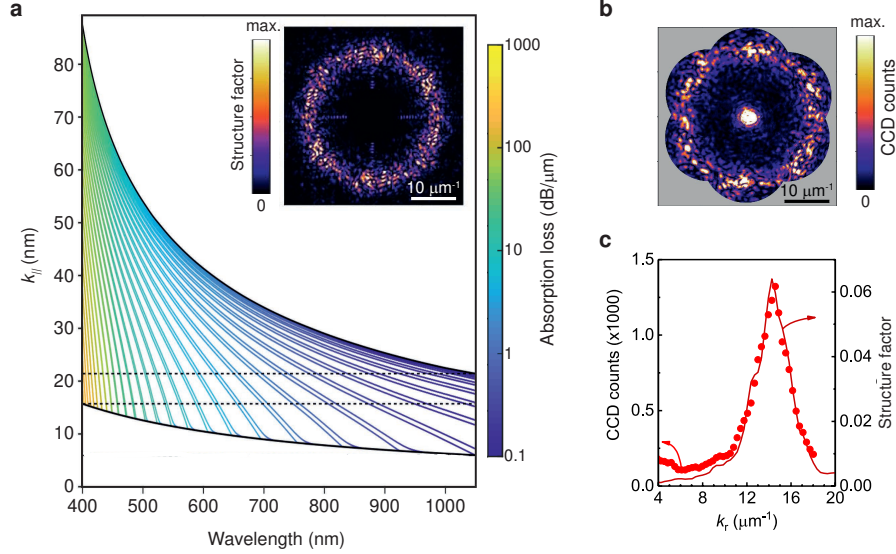


Fig. 2 Light trapping mechanism. **a** Waveguide modes for a homogeneous 1 μm thick Si slab between air and a perfect metal for the wavelength range of interest in a solar cell. The modes are all lossy, with the absorption loss denoted by their color, as shown in the color bar. Black lines denote the dispersion curves for air (lower curve) and for Si (upper curve). The horizontal dashed lines denote two characteristic wavenumbers: $k_1 = 15.71$, and $k_2 = 21.41$ μm⁻¹ as described in the text. Inset: Simulated first order diffraction pattern of the HUD network design that shows a characteristic diffraction ring in the desired k -space. **b** Measured Fourier-space diffraction pattern in reflection of the HUD network lithographically patterned in a Si wafer (wavelength 561 nm). **c** Structure factor based on the radial distribution of the diffraction intensity in **a** and **b**.

128 absorption of the guided modes, coupled-mode theory calculations estimate that the highest
 129 absorption is actually given for uniform diffraction to the k -range from ~ 9 to ~ 25 μm⁻¹
 130 (see the detailed calculation in the Supplementary File). Targeting this wave vector range
 131 is a key design goal for engineering the diffraction pattern.

132 In contrast to periodic and random patterns, hyperuniform designs with correlated dis-
 133 order are an intermediate concept that allows the creation of diffraction into only a tailored
 134 range of wavevectors. In particular, stealthy HUD structures offer a distinctive route to
 135 filling desired bands in Fourier space, intermediate between the continuous k -space content
 136 of random patterns, and the discrete crystal momenta of periodic point patterns. Stealthy
 137 HUD point patterns are isotropic with no diffraction below a certain critical wavevector
 138 value, k_C : $S(k_{||} \leq k_C) = 0$. The so-called stealthiness parameter χ is defined as the frac-

139 tion of wavevectors for which the structure factor vanishes and can be used to measure the
140 hyperuniform correlations. Thus, $\chi = 0$ for purely uncorrelated (Gaussian) point patterns
141 and $\chi > 0.77$ for periodic structures.^{28,36,38,42}

142 Our design approach starts with a 2D HUD point pattern ($\chi \sim 0.4 - 0.5$) that provides
143 the most uniform filling in the Fourier space domain delimited by the two wavenumbers ($k_{\parallel,1}$
144 and $k_{\parallel,2}$) estimated from the waveguide properties of the slab. Once the 2D HUD point
145 pattern is created, it is transformed into a physical 3D design that can be fabricated with
146 two material components: Si and the low refractive index material. In this case, the 2D
147 HUD point pattern is decorated with 200 nm tall Si walls following a Delaunay tessellation
148 protocol³⁸ that form a continuous Si network, and the voids are filled by the low refractive
149 index material. However, with this design light absorption is no longer expected to be
150 optimal as the 3D texture strongly disrupts the waveguide properties of the Si slab. Also,
151 the tessellation protocol causes the resulting 3D network to be nearly hyperuniform as it
152 slightly deviates from hyperuniform,⁵⁶ meaning that its structure factor has some amplitude
153 for $k_{\parallel} < k_c$.

154 To resolve this non-ideality, we introduce a second optimisation step to fine-tune the
155 HUD-based 3D pattern, where the HUD properties (average distance between points) and
156 Si filling fraction are optimised. This is done with full-wave 3D numerical simulations that
157 compute light absorption at each optimisation step (see Methods and Supplementary File).
158 While the process is computationally expensive, the initial 2D HUD optimisation procedure
159 sets a good base to rapidly find a local maximum. As a result, we obtain an optimised 3D
160 structure based on a 2D HUD point pattern, but with a structure factor function that may
161 differ from what was initially estimated from the slab waveguiding properties. The inset
162 in Fig. 2a shows the 2D simulated structure factor of the fully optimised HUD network
163 design that was used to create the sample in Fig. 1. The structure factor for the first order
164 diffraction shows a clear fingerprint of the hyperuniformity with a circular region around
165 $k_{\parallel} = 0$ where $S(k)$ vanishes, but there is not a sharp cut-off as initially imposed. The nearly-

166 hyperuniform structure factor is better discerned in the angle-averaged structure factor (solid
167 curve) shown in Fig. **2c**. Notice that the Fourier space in the optimised pattern is filled in
168 the wavevector region between 12 and 17 μm^{-1} , which is slightly different than the initial
169 guess for $k_{\parallel,1}$ and $k_{\parallel,2}$.

170 We have performed momentum spectroscopy of the fabricated pattern on a Si surface,
171 where the measured k-space diffraction pattern in reflection is shown in Fig. **2b** as obtained
172 using high-NA Fourier microscopy.⁵⁷ By construction the HUD pattern is designed to scatter
173 normally incident light to parallel wave vectors that are *outside* the collection NA of air ob-
174 jectives. However, by combining strongly off normal illumination at six azimuthal angles we
175 can reconstruct the structure factor in 2D Fourier space up to an effective NA almost twice
176 higher than that of the objective lens (see full details in the Methods section). The angle
177 resolved diffraction measured in reflection displays a similar fingerprint of the hyperuniform-
178 mity as the 2D structure factor of the design. The measured angle-averaged reflection is
179 also plotted in Fig. **2c**, and is extremely well reproduced by the theoretical structure factor
180 (solid line).

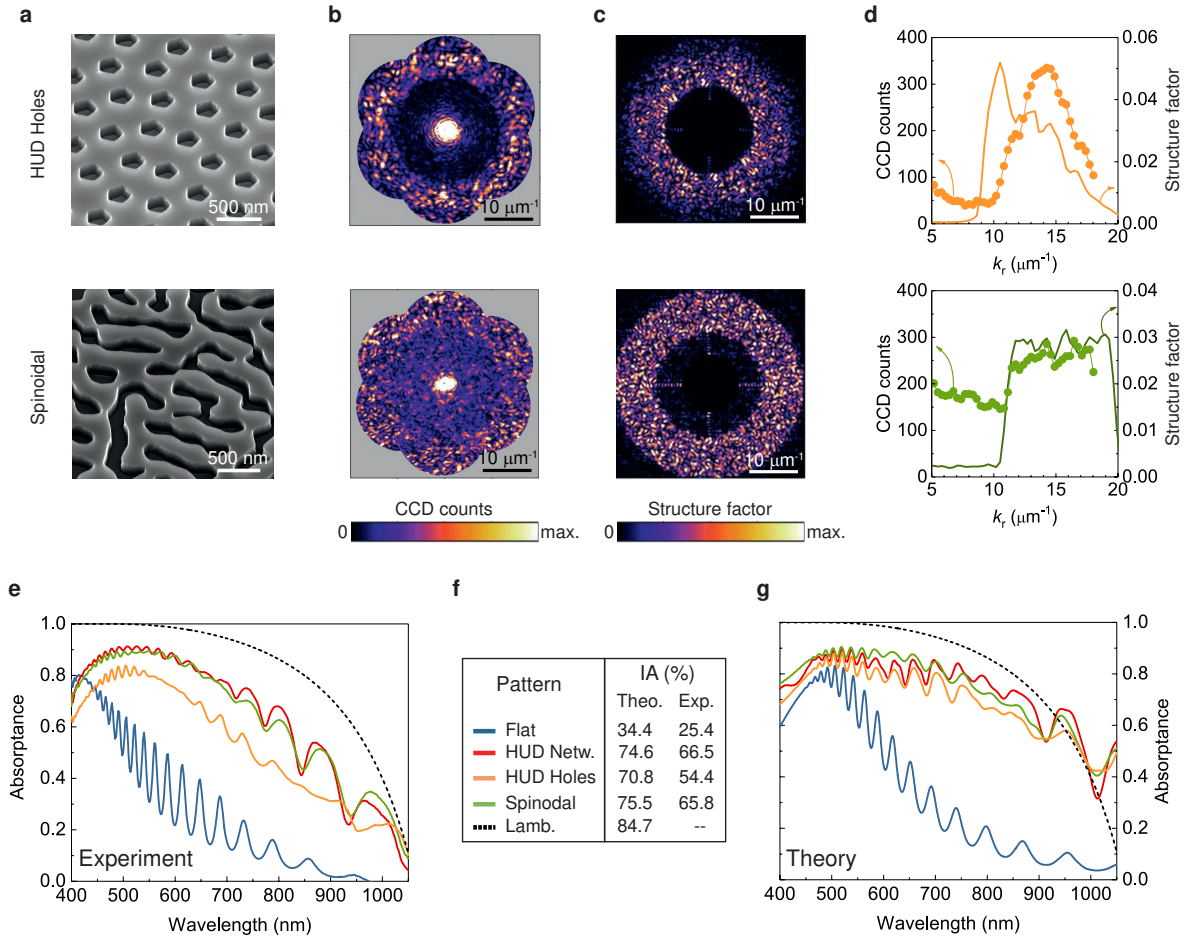


Fig. 3 Performance comparison between different HUD-based designs. **a** SEM images of samples textured with the *HUD hole* (top) and *spinodal* (bottom) designs. **b** Measured angle-resolved diffraction in reflection of the corresponding pattern. **c** Simulated 2D structure factor for the optimised *spinodal* and *HUD hole* patterns. **d** Structure factor as a function of in-plane wavevector (k_r) given by the angle-averaged simulated (solid curve) and measured (dots) diffraction. Measured (**e**) and calculated (**g**) absorptance spectra for a $1\mu\text{m}$ thick Si slab suspended in air with the different surface nanopattern designs with ARC considered. The absorption spectrum for the *HUD network* design is the same as in Fig.1. The theoretical Lambertian limit and the absorption for a flat Si slab (with an ARC) are shown as reference. **f** Table listing the percentage of integrated absorbed solar photons (IA) for all patterns for the wavelength range of 400 – 1050 nm. These numbers are obtained by integrating the theoretical or experimental absorption spectra over the solar flux (AM1.5G) and normalising for the total photon flux in the specified wavelength range.

182 So far, we have shown that a 2D HUD point pattern can lead to a highly efficient 3D design
 183 for broadband light trapping in a thin Si slab, by *decorating* the point pattern with two

184 materials in a wall network fashion (Fig. 1b). However, there are many other decorating
 185 possibilities for the same initial 2D HUD pattern. For instance, instead of the wall network,
 186 one could place Si nano-pillars or nano-holes at the points of the 2D HUD point pattern
 187 and fill the voids with ARC. This is the simplest HUD design, where a single element is
 188 cloned at tailored positions. We refer to this texture as *HUD hole*, and the SEM image of
 189 the as-fabricated sample is shown in Fig. 3a. Similar to the *HUD network* in Fig. 1, the
 190 Fourier microscopy intensity map, Fig. 3(b,top), indicates the HUD nature of the the design
 191 and it is very similar to the theoretical structure factor, Fig. 3(c,top).

192 Another very different way of obtaining 3D HUD patterns is inspired by the generation
 193 of *spinodal* structures.^{58,59} Here the mathematical recipe is to first define a random super-
 194 position of cosine waves with random phase, with wave vectors imposed by the desired wave
 195 vector distribution ($k_{\parallel,1} \leq k_{\parallel} \leq k_{\parallel,2}$), or structure factor. Thresholding the resulting function
 196 at a fixed height value defines material boundaries separating Si and low refractive index
 197 material (filling fraction f set by threshold choice), tracing out zebra-like patterns as in Fig.
 198 3(a, bottom). The resulting two-phase material pattern is nearly hyperuniform, for which its
 199 structure factor is dominated by the wave vector distribution imposed at the initial design
 200 stage. Owing to its inspiration, we refer to this design as *spinodal*. Fourier microscopy of the
 201 as-fabricated *spinodal* design, Fig. 3(b, bottom), also exhibits a characteristic low scattering
 202 at small wavevectors, and a marked increase of scattering at $k_{\parallel} \sim 11 \mu\text{m}^{-1}$. The contrast
 203 is lower compared to the other HUD designs and the scattering at small wavevectors is not
 204 expected from the theoretical structure factor, Fig. 3(c, bottom). We suspect the additional
 205 scattering at low wavevectors arises from fabrication imperfections.

206 The azimuthally-averaged k-space resolved diffraction and theoretical structure factor for
 207 the *HUD holes* and *spinodal* designs are shown in Fig. 3d as dots and solid lines, respectively.
 208 While the intensity distribution in the structure factor of the *HUD holes* is similar in shape
 209 to that of the *HUD network* pattern with a peak at $\approx 15 \mu\text{m}^{-1}$, the structure factor of
 210 the *spinodal* is quite different and resembles a square function. All three proposed designs

211 have a structure factor that is well suited to couple normally incident sunlight into the
212 plane for absorption. The theoretical and experimental absorption spectra for the patterned
213 and unpatterned suspended membranes are shown in Fig. 3e and g, where the ARC (same
214 parameters for all designs) is also taken into account. The spectrum for the *HUD network*
215 pattern is also included and it is the same as in Fig. 1c As a quantitative measure to compare
216 absorption between all the different designs, we have computed the fraction of absorbed solar
217 photons (integrated absorption, IA), as listed in the table in Fig. 3f. The IA, is computed
218 by considering the AM1.5G solar spectrum for the wavelength range of 400 to 1050 nm
219 (see the Methods section for more details). For comparison, we also plot the Lambertian
220 limit obtained by considering the same optical constants used in the full-wave simulations.
221 Similar to the spectra measured in the *HUD network* patterned membrane (red curve), the
222 two new designs raise light absorption in the long wavelength regime, particularly in the
223 case of the *spinodal* (green curve). As expected from the absorption spectra, the *spinodal*
224 and *HUD network* patterns result in a similar IA ($\sim 66\%$ in practice and $\sim 75\%$ in theory).
225 As also predicted by theory, the *HUD holes* design leads to a slightly lower absorption and
226 IA ($\sim 54\%$ in practice and $\sim 70\%$ in theory). We attribute the discrepancy between theory
227 and experiment to local deviations in the ARC and membrane thickness. In any case, for all
228 three designs the measured IA is more than twice that of the unpatterned membrane and
229 we experimentally demonstrate for the first time and for two patterns that absorption is as
230 high as $\sim 78\%$ of the Lambertian limit.

231 **Full device design and efficiency estimation.**

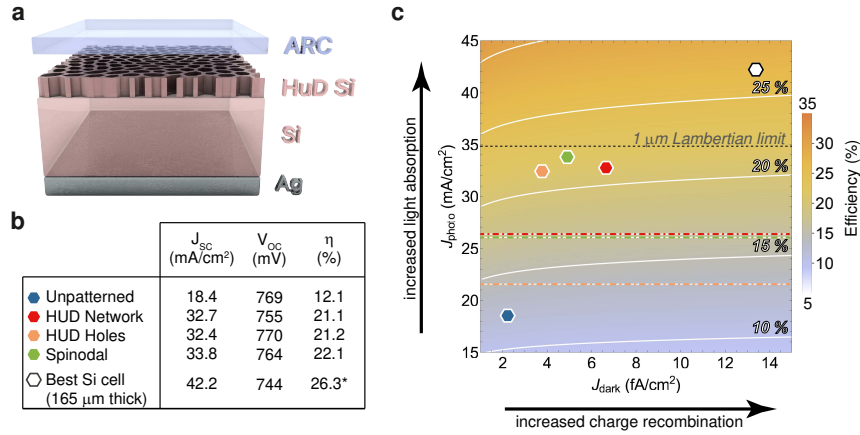


Fig. 4 PV efficiency estimation. **a** Full solar cell device design, which includes a Ag back-contact and improved ARC ($n_{LRM} = 1.82$ and 72 nm thick) **b** Table summarising the estimated PV performance parameters from our optical and PC1D device simulations. **c** Color-map indicating the non-linear dependence of the maximum PV efficiency on the dark and photo-currents (J_{dark} and J_{photo} , respectively). The white lines are isolines at the efficiency indicated by the labels. The dashed black line corresponds to the J_{photo} given by the Lambertian limit in a 1 μ m-thick Si slab. The dash-dotted lines correspond to the J_{photo} derived from our absorption measurements without back-reflector. The data points correspond to the estimated PC1D efficiencies for the different designs. The efficiency estimated for the unpatterned Si membrane and that for the best demonstrated bulk Si cell are shown for comparison. The total efficiency is not only affected by increased light trapping, but also by the additional pattern-induced surface area recombination, reflected in the increased dark current.

232 So far, we have demonstrated the exceptional light trapping properties of the HUD patterns
 233 in thin Si, as evidenced by the enhanced absorption. However, in a full solar cell device
 234 one must also consider other effects of nanotexturing on its performance. It is important
 235 to assure that the gain from light trapping for PV remains despite the potential penalty of
 236 increased surface recombination, which can strongly affect the performance of devices with
 237 a Si thickness smaller than $\sim 90 \mu$ m, where bulk-related losses are negligible. In order to
 238 understand the effects of our HUD-based designs on the PV efficiency, we consider the full
 239 device structure shown in Fig. 4a. Now, the patterned Si film sits on top of a silver metal
 240 contact that also acts as a back reflector. By using interdigitated macroscopic Ag pads, both
 241 the n and p contacts are placed at the rear which reduces shading on the front of the cell.

242 This technology, known as interdigitated back contact (IBC) photovoltaics, has enabled the
243 highest PV efficiency in Si-based cells.⁶⁰⁻⁶² For simplicity, in our absorption calculations we
244 consider a continuous Ag film at the back instead of the interdigitated pads, which is a fair
245 assumption for optical purposes given their large characteristic sizes.

246 We have re-optimised the 3D pattern design taking into account the Ag back-reflector
247 as part of the full structure. We also consider an improved ARC configuration, with
248 $n_{LRM} = 1.82$ and ARC thickness of 72 nm (see Supplementary Information). The resulting
249 absorption spectra for all the different designs are shown in the Supplementary Information.
250 As expected, the metal back-reflector and improved anti-reflection increases light absorption
251 as compared to that shown in Fig. 3g. Interestingly, the three designs offer a highly robust
252 absorption to changes in the angle of incoming light (see the angle dependent absorption
253 spectra in the Supplementary Information file), which strongly enhances the daily PV power
254 output.

255 We have computed the photocurrent, J_{photo} , by integrating the simulated absorbed solar
256 spectrum for the wavelength range of 300 to 1050 nm. To estimate the PV efficiency of our
257 designs we have simulated the current-voltage characteristics of the solar cell with the PC1D
258 software, where we have considered J_{photo} as input and a bulk lifetime of 0.5 ms (standard
259 PV grade Si) and surface recombination velocity (SRV) of 100 cm/s. The SRV value is the
260 state-of-the-art in high efficiency Si solar cell devices.^{1,60} In order to account for the pattern-
261 induced increased surface area, we have considered an effective SRV by multiplying it by
262 the surface area increase factor. A more detailed description of the parameters used in our
263 simulations is given in the Supplementary Information. The table in Fig. 4b summarizes
264 the estimated solar cell performance, in terms of short circuit current (J_{SC}), open circuit
265 potential (V_{OC}) and PV efficiency (η), for the optimised *HUD hole*, *HUD network* and
266 *spinodal* patterns. For comparison, we have included the theoretical case of an unpatterned
267 Si membrane (with ARC) and the current record Si cell, which is 165 μm thick.⁶⁰

268 Because we assume no external resistance losses, $J_{SC} = J_{photo}$. With the pattern-induced

269 light trapping, the J_{SC} in $1\mu\text{m}$ -thick Si is almost doubled for all three designs compared to
 270 the unpatterned cell (from 18.5 mA/cm^2 to 33 mA/cm^2), close to the Lambertian value for 1
 271 μm -thick Si (at 35 mA/cm^2). At the same time, the estimated V_{OC} values in our three designs
 272 are higher than the best bulk cell and oscillate around that expected in an unpatterned thin
 273 film. Because of the small volume in a $1\mu\text{m}$ film compared to bulk, the saturated dark
 274 current, J_{dark} , in the cell is only limited by surface recombination. Considering the state-
 275 of-the-art bulk carrier lifetime and surface recombination velocity, J_{dark} is almost one order
 276 of magnitude smaller in a $1\mu\text{m}$ Si film compared to Si bulk ($165\ \mu\text{m}$ thick) and thus the
 277 V_{OC} is improved by thinning Si down.^{1,5,63} An interesting consequence of this is that lower
 278 grade Si material can thus be used in such thin devices, which have much lower costs (see
 279 the Supplementary Information for more details on how the PV efficiency is affected by the
 280 bulk lifetime and surface recombination). As V_{OC} also depends on the photocurrent, J_{photo} ,
 281 light trapping has the potential to compensate the effects of patterning-induced larger J_{dark}
 282 on the voltage. We find that, the *HUD holes* design uses the smallest surface area and the
 283 strong light trapping fully compensates the effect of increased surface recombination and
 284 leads to the same V_{OC} as in the unpatterned case.

285 From the PC1D full current-voltage characteristics we obtain the PV efficiency. Despite
 286 the different light trapping power and texture design in all three $1\ \mu\text{m}$ -thick Si patterned
 287 cells, we estimate their solar cell efficiency to break the 20% milestone. Fig. 4c represents
 288 the two major consequences of nanotexturing, increased light trapping and increased charge
 289 recombination, on the PV efficiency (color scale) by considering the illuminated diode equa-
 290 tion ($J(V) = J_{dark}(e^{qV/K_B T} - 1) - J_{photo}$). The dashed horizontal black line corresponds to
 291 the ultimate photocurrent from the Lambertian light trapping in $1\ \mu\text{m}$ thick Si and one can see
 292 the span of possible PV efficiencies depending on the carrier recombination properties of the
 293 device. In the graph, we include data points for the unpatterned and the three HUD designs,
 294 based on the J_{photo} and J_{dark} values found in our light absorption and PC1D simulations,
 295 respectively. For comparison, we also include the data point for the best demonstrated Si

296 solar cell, which is 165 μm thick.⁶⁰ Note that the diode equation yields a slightly higher PV
297 efficiency compared to that reported in Ref.60 (0.5% higher efficiency) as the model neglects
298 contact resistance losses. Fig. 4c clearly visualizes the compromise for the total efficiency
299 between light trapping and surface recombination properties of the different designs and it is
300 particularly evidenced by the *HUD holes* and *HUD network*. Despite the fact that the two
301 designs have different light trapping capabilities, the final PV efficiency is very similar.

302 While we theoretically predict the ultimate best device to be that with the *spinodal*
303 texture, the large scale implementation of its fabrication may require some further tech-
304 nological developments. A combination of interference and nanoimprint lithography⁶⁴ has
305 already demonstrated the fabrication of aperiodic structures with defined spatial frequency
306 distribution in areas larger than 1 m^2 . However, further work is needed to increase the
307 required patterning resolution down to few tenths of nanometers. By contrast, HUD point
308 patterns naturally arise in many physical systems, that can lead to simple and scalable fab-
309 rication of the *HUD holes* or *HUD network* patterns. For instance, it has been shown that
310 the structure factor of dispersed colloidal particle (e.g. beads) patterns can be tuned by the
311 ionic strength of the particular solvent^{65,66} and that the dewetting of semiconductor layers
312 leads to HUD patterns.⁶⁷ Also, soft-imprint conformal lithography has proven an excellent
313 low-cost alternative to pattern large-areas with a resolution below 10 nm that could actually
314 serve for both *HUD holes* and *HUD network*.⁶⁸ While a master substrate has to be first made
315 with other lithography methods (such as e-beam lithography), the master can be extensively
316 re-used for the creation of multiple-use soft stamps.

317 Conclusion

318 We have shown that stealthy HUD point patterns are an excellent platform to design a
319 wealth of highly efficient nanoscale textures for trapping light in ultrathin Si solar cells. We
320 have described three different texture designs that offer broadband isotropic light trapping
321 with a characteristic hyperuniform signature in the Fourier reflectance. We have fabricated

322 such textures on a suspended Si membrane and experimentally demonstrated the highest
 323 absorption in 1 μm -thick Si, corresponding to a J_{photo} of 26.3 mA/cm². This exceptional
 324 light trapping can potentially be further improved by optimising the anti-reflection coating
 325 and incorporating a metal back-reflector, which in turn serves as electrical contact. Taking
 326 into account state-of-the-art values of Si electronic properties and IBSC device design, we
 327 estimate realistic PV efficiency above 21% for a 1 μm -thick c-Si cell, which represents a
 328 breakthrough toward flexible, light-weight c-Si PV.

329 **Methods**

330 **Generation of the disordered Hyperuniform structures**

331 A hyperuniform point pattern is a random point pattern in real space for which the number
 332 variance $\sigma^2(R)$ within a spherical sampling window of radius R (in d dimensions) grows more
 333 slowly than the window volume ($\propto R^d$) for large R . We consider point patterns that are
 334 stealthy, which is a property of the structure factor $S(\mathbf{k})$, defined as²⁷

$$S(\mathbf{k}) = \frac{1}{N} \left| \sum_{n=1}^N e^{i\mathbf{k}\cdot\mathbf{r}_n} \right|^2, \quad (1)$$

335 where \mathbf{k} are vectors in reciprocal space and \mathbf{r}_n are the positions of the N particles. For
 336 stealthy point patterns, $S(\mathbf{k})$ is isotropic and vanishes for a finite range of wave numbers $0 <$
 337 $k \leq k_0$, for some positive critical wave vector, k_0 .²⁹ The size of this region can be expressed
 338 through the so-called stealthy parameter $\chi = M(\mathbf{k})/dN$, where $M(\mathbf{k})$ is the number of
 339 linearly independent \mathbf{k} vectors where $S(\mathbf{k}) = 0$ and $d = 2$ in the present case.^{29,38}

340 **Generation of the spinodal pattern**

341 Density wave (spinodal) structures or spinodal structures are a particular realization of
 342 hyperuniform structuring and can be generated according to a simple protocol.⁵⁸ We consider

343 the function

$$\Phi(\mathbf{r}) = \sum_{j=1}^{N_q} \cos(\mathbf{q}_j \cdot \mathbf{r} + \phi_j) , \quad (2)$$

344 where $k_1 < |\mathbf{q}| < k_2$ is a collection of *homogeneously* distributed random N_q wavevectors
345 and ϕ_j are random phases uniformly distributed in the range $(0, 2\pi)$. This function is hy-
346 peruniform by construction with its Fourier transform uniformly distributed in the k-space
347 ring defined by $k_1 < |\mathbf{q}| < k_2$. To obtain a two-phase dielectric function we define

$$\epsilon(\mathbf{r}) = \begin{cases} \epsilon_1 , \Phi(\mathbf{r}) < \Phi_0 \\ \epsilon_2 , \Phi(\mathbf{r}) \geq \Phi_0 \end{cases} , \quad (3)$$

348 where ϵ_1 and ϵ_2 are relevant dielectric permittivities of the two phases, and Φ_0 is a value
349 chosen to yield the desired filling fraction. We note the cut procedure defined above may
350 violate the strict hyperuniformity constraints, and in practice the resulting structures are
351 nearly-hyperuniform with most of the Fourier components concentrated in the k-space ring
352 defined by $k_1 < |\mathbf{q}| < k_2$.

353 Absorption simulations

354 Optical simulations were performed using the a freely available finite-difference time-domain
355 (FDTD) solver.⁶⁹ In all cases, the disordered structures were generated under periodic bound-
356 ary conditions and are modelled as super-cells with sizes between 10 - 15 μm . For absorption
357 simulations, we have employed periodic boundary conditions in the transverse directions
358 and perfect matching layer boundary conditions in the longitudinal direction. The disper-
359 sive dielectric function of Si was modeled using a sum of Lorentzian terms²³ as detailed
360 in the Supplementary Information and the mesh resolution was 5.2 nm. To calculate the
361 absorption, the structure was illuminated by broad bandwidth plane waves pulses, and the
362 subsequent transmitted and reflected fluxes were recorded for a long simulation time. Due to
363 the diffusive character of the wave propagation and presence of various localised resonances

364 in the disordered texture layer, the simulation is not run for a fixed amount of time but it
365 keeps running until the field in the slab have decayed by a factor of 5×10^{-5} from its peak
366 value in an interval of 20 simulation time units.⁶⁹

367 **Sample fabrication**

368 Single crystal $\langle 100 \rangle$ $1\mu\text{m}$ Si membranes (Norcada Inc.) were used. The actual thickness of the
369 membrane may vary slightly. From the Fabry-Pérot interference pattern in the absorption
370 spectrum for the unpatterned membrane nearby the patterned areas, we deduce a total
371 thickness of 1180 nm. The membranes were either $1.3 \times 1.3 \text{ mm}^2$ or $4.8 \times 4.8 \text{ mm}^2$ in size in
372 a Si frame of $10 \times 10 \text{ mm}^2$ and $300 \mu\text{m}$ thick. The nanopatterns were made by electron beam
373 lithography followed by reactive ion etching. First, CSAR e-beam resist was spin coated as
374 mask. Fields of either 100×100 , 150×150 or $180 \times 180\mu\text{m}^2$ patterns were exposed. After
375 exposure and development, 200 nm of the Si membrane was etched by first removing the
376 native oxide followed by HBr and O_2 etching. The left-over resist was lifted off, and the
377 sample was ready for Fourier microscopy. For the absorption measurements, an additional
378 layer of resist (OrmoComp[®] resist) was spin coated on top of the sample to act as anti-
379 reflective coating, ARC. The effects of the ARC on light absorption are described in the
380 Supplementary Information. From the interference fringes in the absorption spectrum taken
381 on the unpatterned area, we deduce that the resist layer is of 200 nm.

382 **Fourier-space illumination and imaging**

383 In order to experimentally characterize the structure factor of the hyperuniform structures,
384 we employed high-NA back focal plane imaging, also known as Fourier microscopy. In
385 this technique angle-dependent scattering patterns of a sample are captured in single shot
386 measurements, as opposed to performing angular scans using a rotation stage. We used
387 a home-built inverted microscope reported in Ref.⁵⁷ that operates in reflection mode, so
388 we chose the structures on the Si wafer for these measurements for easier handling. The

389 microscope is infinity corrected with an Olympus MPlan IR 100x NA=0.95 objective, a 200
390 mm tube lens and 200 mm Fourier lens.

391 As the light source we use a cw DPSS laser (Lasos DPSS) with a wavelength of 561.3
392 nm. At this wavelength, the actual microscope NA equals 0.89, as calibrated with a diffrac-
393 tion grating. The image of the objective back focal plane is relayed to an Andor Clara
394 silicon CCD camera. According to the Abbe sine condition, captured Fourier images di-
395 rectly map parallel momentum space, as scattering at angle θ, ϕ (polar angle relative to
396 sample normal and azimuthal angle, respectively) projects onto the camera plane at location
397 $(x, y) = f_o(\cos \phi \sin \theta, \sin \phi \sin \theta) \propto \mathbf{k}_{\parallel}$, where f_o is the microscope objective focal length
398 ($f=1.8$ mm). Since we essentially measure the structure factor as function of k_{\parallel} (wave vec-
399 tor parallel to the Si/air interface), one would expect to see the same dependence in both
400 reflection and transmission.

401 Essential to our experiment is that the HUD patterns have structure factor $S(\mathbf{k}_{\parallel})$ predom-
402 inantly at parallel momentum *just outside* the NA of our collection objective, corresponding
403 to scattering normally incident light into guided modes. The ring of diffraction intensity
404 distribution in momentum space follows $I(\mathbf{k}_{\parallel}) = S(\mathbf{k}_{\parallel} - \mathbf{k}_{\text{in},\parallel})$ and is therefore centered on
405 the incident parallel momentum $\mathbf{k}_{\text{in},\parallel}$. From free space one can therefore access the structure
406 factor $S(\mathbf{k}_{\parallel})$ for parallel momenta up to *twice* the microscope NA by illuminating at multiple
407 oblique incidence angles [$0 < \frac{|\mathbf{k}_{\text{in},\parallel}|}{2\pi/\lambda} \approx \text{NA}$].

408 In order to access any excitation angle without physically moving parts of the set up,
409 the excitation path is equipped with a spatial light modulator (Meadowlark 1920×1152
410 XY Phase Series SLM) that is imaged onto the microscope back focal plane. By displaying
411 regions of blazed phase gratings on the SLM, light can be selectively send to the first grating
412 order. This allows an effective amplitude modulation, by placing an iris in the Fourier plane
413 of the SLM, which blocks all light except for the modulated first diffraction order.⁷⁰ By
414 displaying a single small circle on the SLM and choosing its position, illumination with
415 arbitrarily $\mathbf{k}_{\text{in},\parallel}$ can be generated. For each structure we collected six images arranged as

416 the vertices of a hexagon. To obtain $S(\mathbf{k}_{\parallel})$ collected images were shifted by their respective
417 $k_{\text{in},\parallel}$, while overlapping image areas were averaged.

418 **Absorption measurements**

419 Absorption measurements on the membrane were done by using an integrating sphere micro-
420 scope (modified LabSphere GPS-020-SL with the 17 mm working distance objective Mitutoyo
421 M Apo Plan NIR 50 \times and NA = 0.42) coupled with a supercontinuum laser (Fianium WL-
422 SC-390-3) and an acousto-optical tunable filter (AOTF, Crystal Technologies, with roughly
423 4 nm bandwidth). The back-scattered and transmitted light are both detected together and
424 by adding the specularly reflected signal, we determine absorption. The photodetectors are
425 Thorlabs amplified Si detectors (PDA100A), read out by Stanford Research Systems SR830
426 lock-in amplifiers. More details about the integrating sphere microscope set-up can be found
427 in Ref. 52 . We have used three photo-detectors to measure the reference beam, the reflected
428 and the transmitted/forward scattered light, respectively. The light reflected back into the
429 objective is detected with the reflection detector, while the integrating sphere detector de-
430 tects the transmitted and scattered light. The absorbance is calculated by subtracting the
431 reflected and transmitted/scattered power from the incident power. Two reference measure-
432 ments in reflection and transmission were done with a glass slide and calibrated mirror, to
433 account for the response function of the set-up.

434 **Acknowledgement**

435 This work is part of the Dutch Research Council (NWO) and was partially performed
436 at the research institute AMOLF. R.S. acknowledges funding by EPSRC (EP/P033431,
437 EP/M013812 and EP/M027961). M.F. acknowledges support from the University of Sur-
438 rey's IAA awards, the EPSRC (United Kingdom) EP/N509772/1, EPSRC (United King-
439 dom) Strategic Equipment Grant No. EP/L02263X/1 (EP/M008576/1) and EPSRC (United

440 Kingdom) Grant EP/M027791/1.

441 The authors thank Julia van der Burgt and Albert Polman for fruitful discussions. Special
442 thanks also to the technical support staff of the AMOLF NanoLab Amsterdam, for their
443 support with sample fabrication.

444 **Author contributions**

445 R.J.S., G.G. C.W. and M.F. carried out the HUD optimisation and optical simulations.
446 N.T., E.K. and R. R. performed the measurements and processed the experimental data.
447 P.K. performed the PC1D simulations. E.A.L., R.S., M.F. and A.F.K. were involved in
448 planning and supervision of the work. E.A.L. and M.F. initiated and directed the project.
449 All authors contributed to writing the manuscript.

450 **Supporting Information Available**

451 A listing of the contents of the Supporting Information file is below:

- 452 • Design parameters
- 453 • Absorption spectra in the full device
- 454 • Silicon dispersion model
- 455 • Mode coupling analysis
- 456 • Angular dependence of absorption
- 457 • PC1D simulation details
- 458 • Bulk lifetime and surface recombination effects

References

- (1) Liu, Z.; Sofia, S. E.; Laine, H. S.; Woodhouse, M.; Wieghold, S.; Peters, I. M.; Buonassisi, T. Revisiting thin silicon for photovoltaics: A technoeconomic perspective. *Energy Environ. Sci.* **2020**, *13*, 12–23.
- (2) Fedorchenko, A. I.; Wang, A. B.; Cheng, H. H. Thickness dependence of nanofilm elastic modulus. *Appl. Phys. Lett.* **2009**, *94*, 152111.
- (3) Wang, S.; Weil, B. D.; Li, Y.; Wang, K. X.; Garnett, E.; Fan, S.; Cui, Y. Large-area free-standing ultrathin single-crystal silicon as processable materials. *Nano Lett.* **2013**, *13*, 4393–4398.
- (4) Bong, J. H.; Kim, C.; Hwang, W. S.; Kim, T. S.; Cho, B. J. A quantitative strain analysis of a flexible single-crystalline silicon membrane. *Appl. Phys. Lett.* **2017**, *110*, 033105.
- (5) Richter, A.; Hermle, M.; Glunz, S. W. Reassessment of the limiting efficiency for crystalline silicon solar cells. *IEEE J. Photovoltaics* **2013**, *3*, 1184–1191.
- (6) Kowalczewski, P.; Andreani, L. C. Towards the efficiency limits of silicon solar cells: How thin is too thin? *Sol. Energy Mater. Sol. Cells* **2015**, *143*, 260–268.
- (7) Polman, A.; Atwater, H. A. Photonic design principles for ultrahigh-efficiency photovoltaics. *Nat. Mater.* **2012**, *11*, 174–177.
- (8) Pala, R. A.; White, J.; Barnard, E.; Liu, J.; Brongersma, M. L. Design of plasmonic thin-film solar cells with broadband absorption enhancements. *Adv. Mater.* **2009**, *21*, 3504–3509.
- (9) Yu, P.; Zhang, F.; Li, Z.; Zhong, Z.; Govorov, A.; Fu, L.; Tan, H.; Jagadish, C.; Wang, Z. Giant optical pathlength enhancement in plasmonic thin film solar cells using core-shell nanoparticles. *J. Phys. D. Appl. Phys.* **2018**, *51*, 295106.

- 483 (10) Raja, W.; Bozzola, A.; Zilio, P.; Miele, E.; Panaro, S.; Wang, H.; Toma, A.; Alabas-
484 tri, A.; De Angelis, F.; Zaccaria, R. P. Broadband absorption enhancement in plasmonic
485 nanoshells-based ultrathin microcrystalline-Si solar cells. *Sci. Rep.* **2016**, *6*, 24539.
- 486 (11) Ferry, V. E.; Sweatlock, L. A.; Pacifici, D.; Atwater, H. A. Plasmonic Nanostructure
487 Design for Efficient Light Coupling into Solar Cells. *Nano Lett.* **2008**, *8*, 4391–4397.
- 488 (12) Chen, H.-L.; Cattoni, A.; De Lépinau, R.; Walker, A. W.; Höhn, O.; Lackner, D.;
489 Siefer, G.; Faustini, M.; Vandamme, N.; Goffard, J.; Behaghel, B.; Dupuis, C.; Bar-
490 dou, N.; Dimroth, F.; Collin, S. A 19.9%-efficient ultrathin solar cell based on a 205-
491 nm-thick GaAs absorber and a silver nanostructured back mirror. *Nat. Energy* **2019**,
492 *4*, 761–767.
- 493 (13) Gomard, G.; Drouard, E.; Letartre, X.; Meng, X.; Kaminski, A.; Fave, A.; Lemiti, M.;
494 Garcia-Caurel, E.; Seassal, C. Two-dimensional photonic crystal for absorption enhance-
495 ment in hydrogenated amorphous silicon thin film solar cells. *J. Appl. Phys.* **2010**, *108*,
496 123102.
- 497 (14) Battaglia, C.; Hsu, C. M.; Söderström, K.; Escarré, J.; Haug, F. J.; Charrière, M.;
498 Boccard, M.; Despeisse, M.; Alexander, D. T.; Cantoni, M.; Cui, Y.; Ballif, C. Light
499 trapping in solar cells: Can periodic beat random? *ACS Nano* **2012**, *6*, 2790–2797.
- 500 (15) Yin, G.; Knight, M. W.; van Lare, M. C.; Solà Garcia, M. M.; Polman, A.; Schmid, M.
501 Optoelectronic Enhancement of Ultrathin $\text{CuIn}_{1-x}\text{Ga}_x\text{Se}_2$ Solar Cells by Nanophotonic
502 Contacts. *Adv. Opt. Mater.* **2017**, *5*, 1600637.
- 503 (16) Jäger, K.; Fischer, M.; van Swaaij, R. A. C. M. M.; Zeman, M. A scattering model for
504 nano-textured interfaces and its application in opto-electrical simulations of thin-film
505 silicon solar cells. *J. Appl. Phys.* **2012**, *111*, 083108.
- 506 (17) Martins, E. R.; Li, J.; Liu, Y.; Depauw, V.; Chen, Z.; Zhou, J.; Krauss, T. F. De-

- 507 terministic quasi-random nanostructures for photon control. *Nat. Commun.* **2013**, *4*,
508 2665.
- 509 (18) Vynck, K.; Burrese, M.; Riboli, F.; Wiersma, D. S. Photon management in two-
510 dimensional disordered media. *Nat. Mater.* **2012**, *11*, 1017–1022.
- 511 (19) Oskooi, A.; Favuzzi, P. A.; Tanaka, Y.; Shigeta, H.; Kawakami, Y.; Noda, S. Partially
512 disordered photonic-crystal thin films for enhanced and robust photovoltaics. *Appl.*
513 *Phys. Lett.* **2012**, *100*, 181110.
- 514 (20) Ferry, V. E.; Verschuuren, M. A.; Lare, M. C. V.; Schropp, R. E.; Atwater, H. A.;
515 Polman, A. Optimized spatial correlations for broadband light trapping nanopatterns
516 in high efficiency ultrathin film a-Si:H solar cells. *Nano Lett.* **2011**, *11*, 4239–4245.
- 517 (21) Van Lare, C.; Lenzenmann, F.; Verschuuren, M. A.; Polman, A. Dielectric Scattering
518 Patterns for Efficient Light Trapping in Thin-Film Solar Cells. *Nano Lett.* **2015**, *15*,
519 4846–4852.
- 520 (22) Yu, S.; Wang, C.; Zhang, Y.; Dong, B.; Jiang, Z.; Chen, X.; Chen, W.; Sun, C. De-
521 sign of Non-Deterministic Quasi-random Nanophotonic Structures Using Fourier Space
522 Representations. *Sci. Rep.* **2017**, *7*, 3752.
- 523 (23) Pratesi, F.; Burrese, M.; Riboli, F.; Vynck, K.; Wiersma, D. S. Disordered photonic
524 structures for light harvesting in solar cells. *Opt. Express* **2013**, *21*, A460.
- 525 (24) Siddique, R. H.; Donie, Y. J.; Gomard, G.; Yalamanchili, S.; Merdzhanova, T.; Lem-
526 mer, U.; Hölscher, H. Bioinspired phase-separated disordered nanostructures for thin
527 photovoltaic absorbers. *Sci. Adv.* **2017**, *3*, e1700232.
- 528 (25) Bozzola, A.; Liscidini, M.; Andreani, L. C. Broadband light trapping with disordered
529 photonic structures in thin-film silicon solar cells. *Prog. Photovoltaics Res. Appl.* **2014**,
530 *22*, 1237–1245.

- 531 (26) Trevino, J.; Forestiere, C.; Di Martino, G.; Yerci, S.; Priolo, F.; Dal Negro, L.
532 Plasmonic-photonic arrays with aperiodic spiral order for ultra-thin film solar cells.
533 *Opt. Express* **2012**, *20*, A418.
- 534 (27) Torquato, S.; Stillinger, F. H. Local density fluctuations, hyperuniformity, and order
535 metrics. *Phys. Rev. E - Stat. Physics, Plasmas, Fluids, Relat. Interdiscip. Top.* **2003**,
536 *68*, 41113.
- 537 (28) Uche, O. U.; Stillinger, F. H.; Torquato, S. Constraints on collective density variables:
538 Two dimensions. *Phys. Rev. E - Stat. Physics, Plasmas, Fluids, Relat. Interdiscip. Top.*
539 **2004**, *70*, 9.
- 540 (29) Batten, R. D.; Stillinger, F. H.; Torquato, S. Classical disordered ground states: Super-
541 ideal gases and stealth and equi-luminous materials. *J. Appl. Phys.* **2008**, *104*, 33504.
- 542 (30) Castro-Lopez, M.; Gaio, M.; Sellers, S.; Gkantzounis, G.; Florescu, M.; Sapienza, R.
543 Reciprocal space engineering with hyperuniform gold disordered surfaces. *APL Photon.*
544 **2017**, *2*, 174–7.
- 545 (31) Gabrielli, A.; Labini, F. S.; Joyce, M.; Pietronero, L. *Stat. Phys. Cosm. Struct.*;
546 Springer-Verlag: Berlin/Heidelberg, 2005; pp 1–424.
- 547 (32) Zhang, G.; Martelli, F.; Torquato, S. The structure factor of primes. *J. Phys. A Math.*
548 *Theor.* **2018**, *51*, 115001.
- 549 (33) Lei, Q. L.; Ni, R. Hydrodynamics of random-organizing hyperuniform fluids. *PNAS*
550 **2019**, *116*, 22983–22989.
- 551 (34) Mann, S. A.; Sciacca, B.; Zhang, Y.; Wang, J.; Kontoleta, E.; Liu, H.; Garnett, E. C.
552 Integrating Sphere Microscopy for Direct Absorption Measurements of Single Nanos-
553 tructures. *ACS Nano* **2017**, *11*, 1412–1418.

- 554 (35) Wang, J.; Schwarz, J. M.; Paulsen, J. D. Hyperuniformity with no fine tuning in sheared
555 sedimenting suspensions. *Nat. Commun.* **2018**, *9*, 1–7.
- 556 (36) Froufe-Pérez, L. S.; Engel, M.; Sáenz, J. J.; Scheffold, F. Band gap formation and
557 Anderson localization in disordered photonic materials with structural correlations.
558 *PNAS* **2017**, *114*, 9570–9574.
- 559 (37) Ricouvrier, J.; Pierrat, R.; Carminati, R.; Tabeling, P.; Yazhgur, P. Optimizing Hyper-
560 uniformity in Self-Assembled Bidisperse Emulsions. *Phys. Rev. Lett.* **2017**, *119*, 208001.
- 561 (38) Florescu, M.; Torquato, S.; Steinhardt, P. J. Designer disordered materials with large,
562 complete photonic band gaps. *PNAS* **2009**, *106*, 20658–20663.
- 563 (39) Froufe-Pérez, L. S.; Engel, M.; Damasceno, P. F.; Muller, N.; Haberko, J.; Glotzer, S. C.;
564 Scheffold, F. Role of Short-Range Order and Hyperuniformity in the Formation of Band
565 Gaps in Disordered Photonic Materials. *Phys. Rev. Lett.* **2016**, *117*, 053902.
- 566 (40) Tsitrin, S.; Williamson, E. P.; Amoah, T.; Nahal, G.; Chan, H. L.; Florescu, M.;
567 Man, W. Unfolding the band structure of non-crystalline photonic band gap materials.
568 *Sci. Rep.* **2015**, *5*, 13301.
- 569 (41) Leseur, O.; Pierrat, R.; Carminati, R. High-density hyperuniform materials can be
570 transparent. *Optica* **2016**, *3*, 763–767.
- 571 (42) Gorsky, S.; Britton, W. A.; Chen, Y.; Montaner, J.; Lenef, A.; Raukas, M.; Dal Negro, L.
572 Engineered hyperuniformity for directional light extraction. *APL Photon.* **2019**, *4*,
573 110801.
- 574 (43) Milošević, M. M.; Man, W.; Nahal, G.; Steinhardt, P. J.; Torquato, S.; Chaikin, P. M.;
575 Amoah, T.; Yu, B.; Mullen, R. A.; Florescu, M. Hyperuniform disordered waveguides
576 and devices for near infrared silicon photonics. *Sci. Rep.* **2019**, *9*, 1–11.

- 577 (44) Man, W.; Florescu, M.; Williamson, E. P.; He, Y.; Hashemizad, S. R.; Leung, B. Y.;
578 Liner, D. R.; Torquato, S.; Chaikin, P. M.; Steinhardt, P. J. Isotropic band gaps and
579 freeform waveguides observed in hyperuniform disordered photonic solids. *PNAS* **2013**,
580 *110*, 15886–15891.
- 581 (45) Amoah, T.; Florescu, M. High- Q optical cavities in hyperuniform disordered materials.
582 *Phys. Rev. B - Condens. Matter Mater. Phys.* **2015**, *91*, 020201.
- 583 (46) Ma, T.; Guerboukha, H.; Girard, M.; Squires, A. D.; Lewis, R. A.; Skorobogatiy, M.
584 3D Printed Hollow-Core Terahertz Optical Waveguides with Hyperuniform Disordered
585 Dielectric Reflectors. *Adv. Opt. Mater.* **2016**, *4*, 2085–2094.
- 586 (47) Zhou, W.; Tong, Y.; Sun, X.; Tsang, H. K. Hyperuniform disordered photonic bandgap
587 polarizers. *J. Appl. Phys.* **2019**, *126*, 113106.
- 588 (48) PALIK, E. D., Ed. *Handb. Opt. Constants Solids*; Academic Press: Boston, 1998; p iii.
- 589 (49) Ghiradella, H. Light and color on the wing: structural colors in butterflies and moths.
590 *Appl. Opt.* **1991**, *30*, 3492.
- 591 (50) Gissibl, T.; Wagner, S.; Sykora, J.; Schmid, M.; Giessen, H. Refractive index measure-
592 ments of photo-resists for three-dimensional direct laser writing. *Opt. Mater. Express*
593 **2017**, *7*, 2293.
- 594 (51) Mann, S. A.; Oener, S. Z.; Cavalli, A.; Haverkort, J. E.; Bakkers, E. P.; Garnett, E. C.
595 Quantifying losses and thermodynamic limits in nanophotonic solar cells. *Nat. Nan-*
596 *otech.* **2016**, *11*, 1071–1075.
- 597 (52) Mann, S. A.; Sciacca, B.; Zhang, Y.; Wang, J.; Kontoleta, E.; Liu, H.; Garnett, E. C.
598 Integrating Sphere Microscopy for Direct Absorption Measurements of Single Nanos-
599 tructures. *ACS Nano* **2017**, *11*, 1412–1418.

- 600 (53) Depauw, V.; Trompoukis, C.; Massiot, I.; Chen, W.; Dmitriev, A.; Roca I Cabarro-
601 cas, P.; Gordon, I.; Poortmans, J. Sunlight-thin nanophotonic monocrystalline silicon
602 solar cells. *Nano Futur.* **2017**, *1*, 021001.
- 603 (54) Bozzola, A.; Liscidini, M.; Andreani, L. C. Broadband light trapping with disordered
604 photonic structures in thin-film silicon solar cells. *Prog. Photovolt: Res. Appl.* **2014**,
605 *22*, 1237–1245.
- 606 (55) Li, J.; Li, K.; Schuster, C.; Su, R.; Wang, X.; Borges, B. H. V.; Krauss, T. F.; Mar-
607 tins, E. R. Spatial resolution effect of light coupling structures. *Sci. Rep.* **2015**, *5*,
608 18500.
- 609 (56) Hejna, M.; Steinhardt, P. J.; Torquato, S. Nearly hyperuniform network models of
610 amorphous silicon. *Phys. Rev. B - Condens. Matter Mater. Phys.* **2013**, *87*, 245204.
- 611 (57) Schokker, A. H.; Koenderink, A. F. Lasing at the band edges of plasmonic lattices.
612 *Phys. Rev. B - Condens. Matter Mater. Phys.* **2014**, *90*, 155452.
- 613 (58) Teubner, M. Level Surfaces of Gaussian Random Fields and Microemulsions. *Europhys.*
614 *Lett.* **1991**, *14*, 403–408.
- 615 (59) Ma, Z.; Torquato, S. Random scalar fields and hyperuniformity. *J. Appl. Phys.* **2017**,
616 *121*, 244904.
- 617 (60) Yoshikawa, K.; Kawasaki, H.; Yoshida, W.; Irie, T.; Konishi, K.; Nakano, K.; Uto, T.;
618 Adachi, D.; Kanematsu, M.; Uzu, H.; Yamamoto, K. Silicon heterojunction solar cell
619 with interdigitated back contacts for a photoconversion efficiency over 26%. *Nat. Energy*
620 **2017**, *2*, 1–8.
- 621 (61) Jeong, S.; McGehee, M. D.; Cui, Y. All-back-contact ultra-thin silicon nanocone solar
622 cells with 13.7% power conversion efficiency. *Nat. Commun.* **2013**, *4*, 1–7.

- 623 (62) Tomasi, A.; Paviet-Salomon, B.; Jeangros, Q.; Haschke, J.; Christmann, G.; Bar-
624 raud, L.; Descoeurdes, A.; PeterSeif, J.; Nicolay, S.; Despeisse, M.; De Wolf, S.; Ballif, C.
625 Simple processing of back-contacted silicon heterojunction solar cells using selective-
626 area crystalline growth. *Nat. Energy* **2017**, *2*, 17062.
- 627 (63) Sai, H.; Umishio, H.; Matsui, T.; Nunomura, S.; Kawatsu, T.; Takato, H.; Matsub-
628 ara, K. Impact of silicon wafer thickness on photovoltaic performance of crystalline
629 silicon heterojunction solar cells. *Jpn. J. Appl. Phys.* 2018.
- 630 (64) Bläsi, B.; Tucher, N.; Höhn, O.; Kübler, V.; Kroyer, T.; Wellens, C.; Hauser, H. Large
631 area patterning using interference and nanoimprint lithography. *Micro-Optics 2016*
632 **2016**, 9888, 98880H.
- 633 (65) Donie, Y. J.; Smeets, M.; Egel, A.; Lentz, F.; Preinfalk, J. B.; Mertens, A.; Smirnov, V.;
634 Lemmer, U.; Bittkau, K.; Gomard, G. Light trapping in thin film silicon solar cells: Via
635 phase separated disordered nanopillars. *Nanoscale* **2018**, *10*, 6651–6659.
- 636 (66) Piechulla, P. M.; Muehlenbein, L.; Wehrspohn, R. B.; Nanz, S.; Abass, A.; Rock-
637 stuhl, C.; Sprafke, A. Fabrication of Nearly-Hyperuniform Substrates by Tailored Dis-
638 order for Photonic Applications. *Adv. Opt. Mater.* **2018**, *6*, 1–10.
- 639 (67) Salvalaglio, M.; Bouabdellaoui, M.; Bollani, M.; Benali, A.; Favre, L.; Claude, J.-B.;
640 Wenger, J.; de Anna, P.; Intonti, F.; Voigt, A.; Abbarchi, M. Hyperuniform monocrys-
641 talline structures by spinodal solid-state dewetting. 2019.
- 642 (68) Verschuuren, M. A.; Knight, M. W.; Megens, M.; Polman, A. Nanoscale spatial lim-
643 itations of large-area substrate conformal imprint lithography. *Nanotech.* **2019**, *30*,
644 345301.
- 645 (69) Oskooi, A. F.; Roundy, D.; Ibanescu, M.; Bermel, P.; Joannopoulos, J. D.; John-
646 son, S. G. Meep: A flexible free-software package for electromagnetic simulations by
647 the FDTD method. *Computer Physics Communications* **2010**, *181*, 687–702.

648 (70) Davis, J. A.; Cottrell, D. M.; Campos, J.; Yzuel, M. J.; Moreno, I. Encoding amplitude
649 information onto phase-only filters. *Appl. Opt.* **1999**, *38*, 5004.

Figures

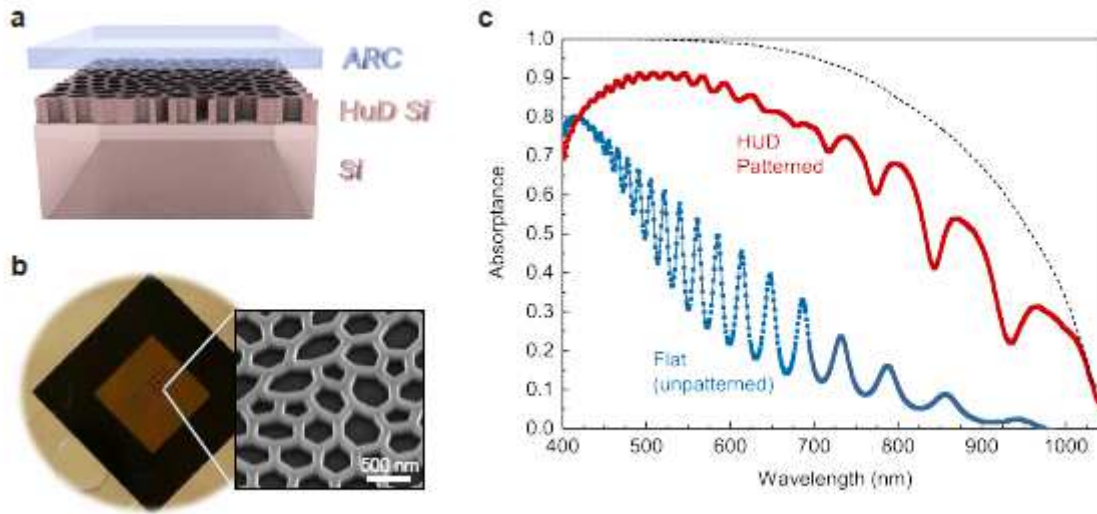


Figure 1

Ultra-thin light absorber design. a Schematic representation of the ultra-thin light absorber consisting of a 1 μm -thick silicon film with the HUD pattern on the top surface (\approx 200 nm thick) to improve light trapping. The pattern is infiltrated with a lower refractive index material (nLRM), which is also used in a top flat layer, ARC, to reduce reflectance (50-100 nm in thickness). Note that the ARC layer is depicted floating above the nanopattern in the image only for clarity purposes b Optical image of the silicon membrane sample supported by a thick silicon frame (1 \times 1 cm²), where the textures have been fabricated. Inset: Scanning electron image of the as-fabricated Si membrane with the optimized honeycomb-like HUD network pattern. c Absorbance spectra measured for the Si membrane with (red) and without (blue) the HUD pattern with ARC. The membrane is suspended in air and infiltrated with a polymer resist (nLRM = 1.52) as ARC. The dashed black line corresponds to the Lambertian limit absorption for 1 μm Si, based on the optical properties given in Ref. 48.

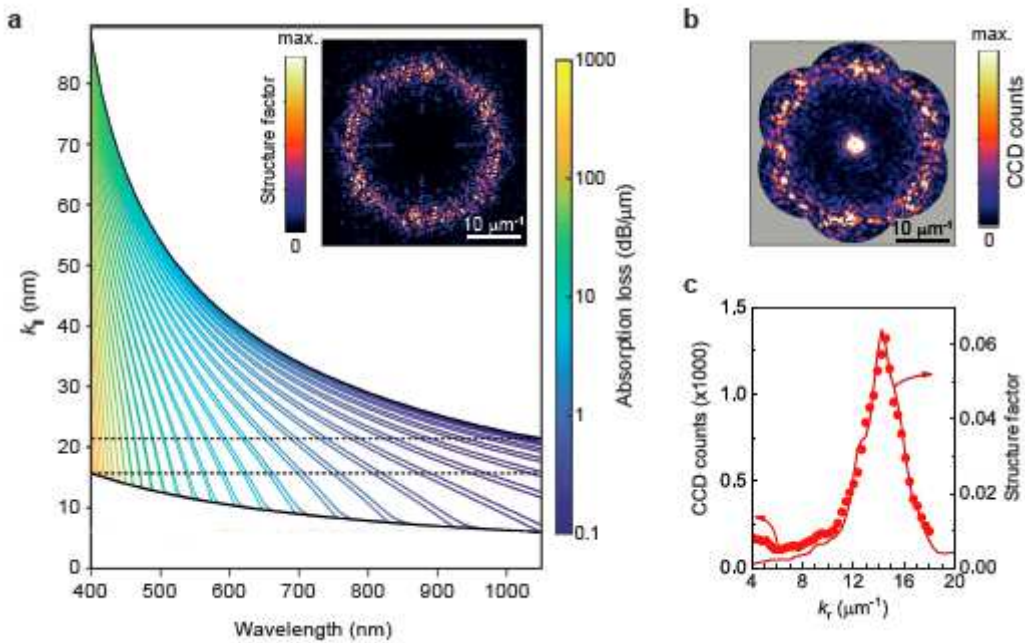


Figure 2

Light trapping mechanism. a Waveguide modes for a homogeneous 1 μm thick Si slab between air and a perfect metal for the wavelength range of interest in a solar cell. The modes are all lossy, with the absorption loss denoted by their color, as shown in the color bar. Black lines denote the dispersion curves for air (lower curve) and for Si (upper curve). The horizontal dashed lines denote two characteristic wavenumbers: $k_1 = 15.71$, and $k_2 = 21.41$ μm⁻¹ as described in the text. Inset: Simulated first order diffraction pattern of the HUD network design that shows a characteristic diffraction ring in the desired k -space. b Measured Fourier-space diffraction pattern in reflection of the HUD network design lithographically patterned in a Si wafer (wavelength 561 nm). c Structure factor based on the radial distribution of the diffraction intensity in a and b.

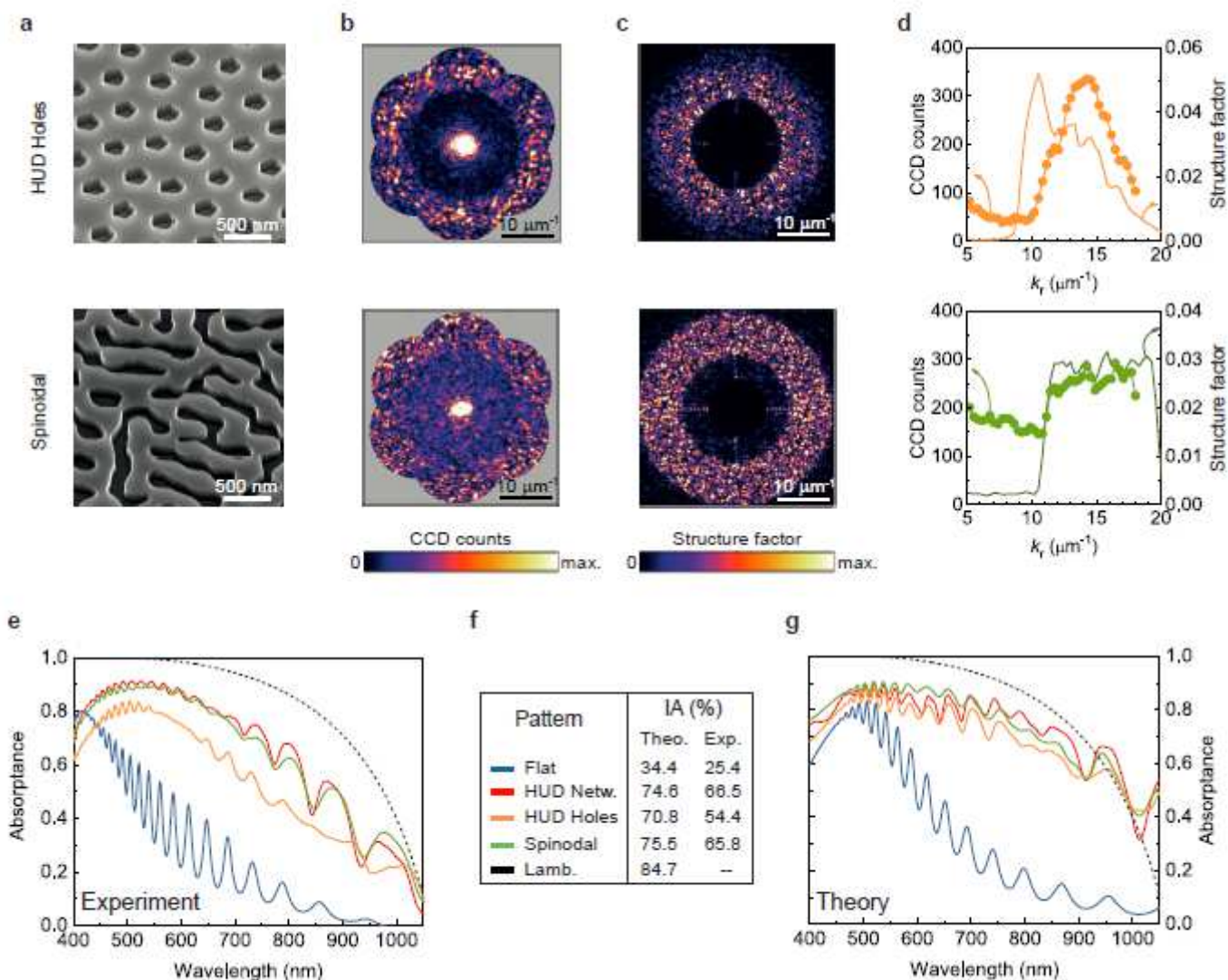


Figure 3

Performance comparison between different HUD-based designs. a SEM images of samples textured with the HUD hole (top) and spinodal (bottom) designs. b Measured angle-resolved diffraction in reflection of the corresponding pattern. c Simulated 2D structure factor for the optimised spinodal and HUD hole patterns. d Structure factor as a function of in-plane wavevector (k_r) given by the angle-averaged simulated (solid curve) and measured (dots) diffraction. Measured (e) and calculated (g) absorbance spectra for a 1 μm thick Si slab suspended in air with the different surface nanopattern designs with ARC considered. The absorption spectrum for the HUD network design is the same as in Fig.1. The theoretical Lambertian limit and the absorption for a flat Si slab (with an ARC) are shown as reference. f Table listing the percentage of integrated absorbed solar photons (IA) for all patterns for the wavelength range of 400 – 1050 nm. These numbers are obtained by integrating the theoretical or experimental absorption spectra over the solar flux (AM1.5G) and normalising for the total photon flux in the specified wavelength range.

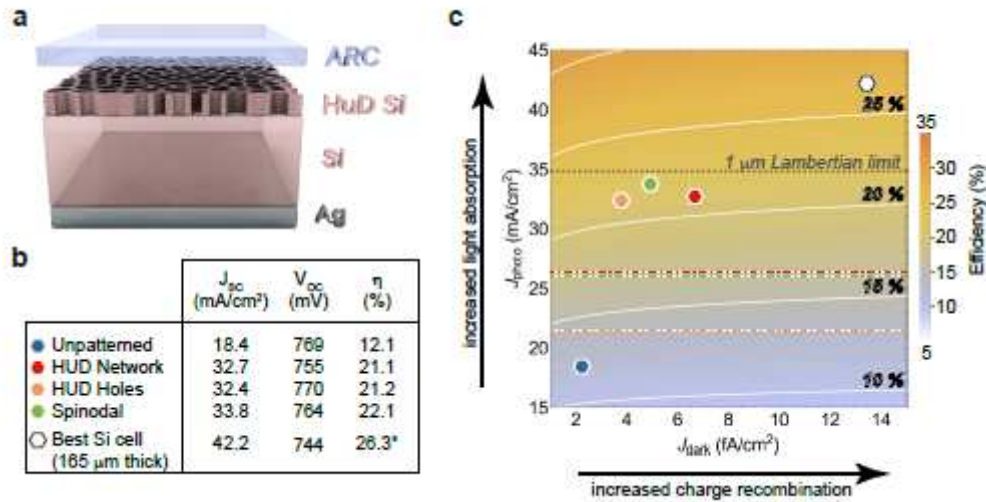


Figure 4

PV efficiency estimation. a Full solar cell device design, which includes a Ag back-contact and improved ARC ($n_{LRM} = 1.82$ and 72 nm thick) b Table summarising the estimated PV performance parameters from our optical and PC1D device simulations. c Color-map indicating the non-linear dependence of the maximum PV efficiency on the dark and photo-currents (J_{dark} and J_{photo} , respectively). The white lines are isolines at the efficiency indicated by the labels. The dashed black line corresponds to the J_{photo} given by the Lambertian limit in a 1 μ m-thick Si slab. The dash-dotted lines correspond to the J_{photo} derived from our absorption measurements without back-reflector. The data points correspond to the estimated PC1D efficiencies for the different designs. The efficiency estimated for the unpatterned Si membrane and that for the best demonstrated bulk Si cell are shown for comparison. The total efficiency is not only affected by increased light trapping, but also by the additional pattern-induced surface area recombination, reflected in the increased dark current.

Supplementary Files

This is a list of supplementary files associated with this preprint. Click to download.

- [HuDSIFinal.pdf](#)